

# Tensile Properties of Some Copper- and Zinc-Based Alloys: Effects of Strain Rate and Test Temperature

B.K. Prasad, A.K. Patwardhan, and A.H. Yegneswaran

(Submitted 18 June 1999)

This study analyzes the effects of test temperature and strain rate on the tensile properties of some copper- and zinc-based alloys. The copper-based alloys comprised a leaded-tin and an aluminum bronze, whereas the zinc-based alloys were added with various quantities of aluminum. The aluminum bronze attained maximum room-temperature tensile strength, whereas that of the leaded-tin bronze was the least. Among the zinc-based alloys, the one comprising 27.5 mass% aluminum exhibited superior tensile strength, followed by those alloyed with 11.5, 37.5, and 47.5 mass% aluminum in a descending order. Increasing strain rate tended to improve the tensile strength of the alloys. Tensile strength was reduced with an increase in test temperature irrespective of the alloy composition. The aluminum bronze possessed maximum strength regardless of temperature. The leaded-tin bronze attained least strength property at low temperatures, whereas higher test temperatures led to superior strength than the zinc-based alloys. The temperature sensitivity of the strength of the zinc-based alloys decreased with their aluminum content. Tensile elongation of the alloys tended to increase with an increase in strain rate and test temperature. Leaded-tin bronze was least affected in either case. The alloy also attained least elongation irrespective of test conditions. The aluminum bronze showed maximum elongation, at least at high strain rates. In the case of the zinc-based alloys, intermediate range of aluminum concentration led to better elongation. The elongation property of the alloys was affected by temperature in different manners. In a few cases, the elongation initially increased followed by a reduction beyond a specific test temperature, whereas, in other cases, a continuous increase with temperature was noted. The observations made have been discussed in terms of the nature of different microconstituents of the alloys whose effectiveness changes with test conditions. The response of the samples has been further substantiated with their fractographic features and subsurface characteristics.

**Keywords** copper-based alloys, microstructure-property correlation, strain rate, tensile properties, test temperature, zinc-based alloys

## 1. Introduction

Bronzes (copper-based alloys) have been in use in different engineering applications since long ago. In many cases, the bronzes comprise costly alloying elements such as lead and tin in a considerable quantity.<sup>[1–4]</sup> Further, health hazards have been reported during the melting of such bronzes.<sup>[5]</sup> Accordingly, attempts have been made to think of suitable, as well as feasible, substitutes for the bronzes.<sup>[5]</sup> Zinc-based alloys have emerged as potential cost- and energy-effective substitutes for the conventionally used bronzes.<sup>[2,5,6]</sup> However, in spite of great potential in this direction, limited efforts have been made to explore the possibilities of replacing bronzes with zinc-based alloys comprising 8 to 28 mass% Al, along with 1 to 3 mass% Cu and ~0.05 mass% Mg,<sup>[2,5,6]</sup> due to a lack of information related to the properties of the zinc-based alloys.<sup>[5]</sup> It should be mentioned that aluminum is one of the major alloying elements in zinc-based alloys that greatly controls the properties of the alloy system.

In view of the above, an attempt has been made to synthesize zinc-based alloys having various concentrations (11.5 to 47.5 mass%) of aluminum and to characterize their tensile properties at different strain rates and test temperatures. The properties of the zinc-based alloys have been compared with those of conventionally used bronzes. The behavior of the alloys has also been explained on the basis of their microstructural features and substantiated with the characteristics of the fractured surfaces and subsurface regions.

## 2. Experimental

### 2.1 Alloy Preparation

Alloys were prepared by liquid metallurgy route in the form of 20 mm diameter, 150 mm long cylindrical castings using cast iron molds. Table 1 represents the chemical composition of the alloys.

### 2.2 Microstructural Characterization

Microstructural studies were carried out on 15 mm thick specimens after polishing them metallographically. The bronzes and the zinc-based alloys were etched with potassium dichromate and diluted aqua regia, respectively. A Leitz (Germany) optical microscope was used for characterizing the samples.

B.K. Prasad and A.H. Yegneswaran, Regional Research Laboratory (CSIR), Habibganj Naka, Bhopal - 462026, India; and A.K. Patwardhan, Metallurgical Engineering Department, University of Roorkee, Roorkee - 247 667, India.

**Table 1 Chemical composition of the experimental alloys**

Serial No.	Specimen	Element, mass%						
		Cu	Sn	Pb	Zn	Al	Fe	Mg
1	Leaded-tin bronze	(a)	7.2	7.3	2.9	...	...	...
2	Aluminum bronze	(a)	...	...	...	9.9	1.2	...
3	Zinc-based alloy 1	2.5	...	...	(a)	11.5	...	0.03
4	Zinc-based alloy 2	2.5	...	...	(a)	27.5	...	0.03
5	Zinc-based alloy 3	2.5	...	...	(a)	37.5	...	0.03
6	Zinc-based alloy 4	2.5	...	...	(a)	47.5	...	0.03

(a) Remainder

### 2.3 Tensile Tests

Tensile strength and elongation of the alloys were evaluated at different test temperatures (308, 333, 373, 423, and 473 K) at typical strain rates of  $1.52 \times 10^{-3} \text{ s}^{-1}$  and strain rates ( $3.8 \times 10^{-4}$ ,  $1.52 \times 10^{-3}$ ,  $1.52 \times 10^{-2}$ , and  $1.52 \times 10^{-1} \text{ s}^{-1}$ ) at ambient temperature (308 K). The test samples had 4 mm gauge diameter and 22 mm gauge length. An Instron (England, U.K.) universal testing machine was used for conducting the tensile tests. The data points represent an average of three observations.

### 2.4 Characterization of Fractured Surfaces and Subsurface Regions

Fractured surfaces and subsurface regions of typical samples were studied using a JEOL 35 CF scanning electron microscope (SEM, Japan Electron Optics Ltd., Tokyo). The specimens were mounted on brass studs and sputtered with gold prior to their SEM examination. Transverse (fractured) sections were mounted in polyester resin and polished according to standard metallographic techniques. This procedure was followed by etching the specimens with diluted aqua regia before mounting them on the studs.

## 3. Results

### 3.1 Microstructural Features

Figure 1 shows the microstructural characteristics of the alloys. The leaded-tin bronze revealed the presence of primary  $\alpha$  dendrites, Cu-Sn intermetallic compound, and discrete particles of lead (Fig. 1a, regions marked A, B, and C, respectively), whereas the aluminum bronze exhibited primary  $\alpha$  dendrites surrounded by Cu-Al phase and particles of iron (Fig. 1b, regions marked A, D, and single arrow, respectively). Important microconstituents of the zinc-based alloy with 11.5 mass% Al were primary  $\alpha$  dendrites and eutectic  $\alpha + \eta$  (Fig. 1c, regions marked A and E, respectively). The zinc-based alloys comprising higher concentrations of aluminum showed features (Fig. 1d through f) identical to Fig. 1(c), except that eutectoid  $\alpha + \eta$  was observed in the former case (Fig. 1d through f, regions marked F) in place of the eutectic  $\alpha + \eta$  (Fig. 1c, region marked E). Metastable  $\epsilon$  phase was also noticed in all the zinc-based alloys (Fig. 1d through f, double-arrow marked

regions). Microstructural aspects of the alloys have been discussed elsewhere.<sup>[7-11]</sup>

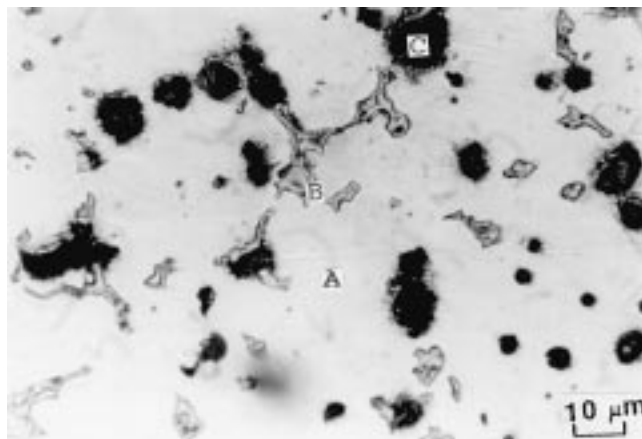
### 3.2 Tensile Properties

Figure 2 represents the tensile strength of the alloys as a function of strain rate and test temperature. The strength increased with strain rate (Fig. 2a). Further, the aluminum bronze attained maximum strength, whereas that of the leaded-tin bronze was the least irrespective of the strain rate. Among the zinc-based alloys, the one comprising 27.5 mass% Al attained maximum strength followed by those having 11.5, 37.5, and 47.5 mass% Al in a descending order (Fig. 2a).

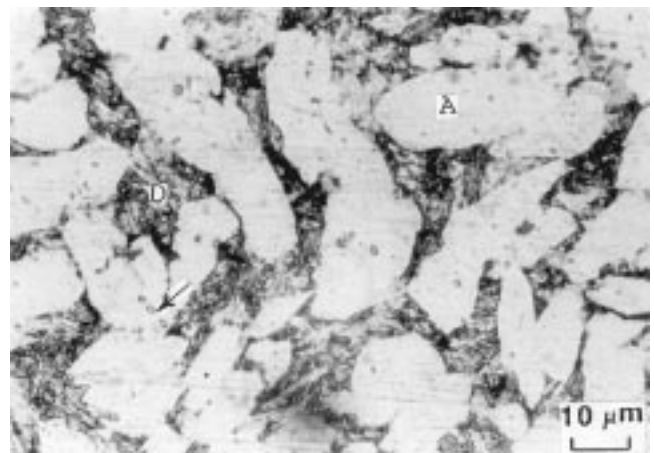
Increasing test temperature deteriorated the strength property of the specimens (Fig. 2b). Moreover, the extent of reduction in the case of the bronzes was noted to be considerably less than the zinc-based alloys (Fig. 2b). The aluminum bronze exhibited maximum strength over the entire range of test temperatures. In the case of the leaded-tin bronze, strength was less than the zinc-based alloys at low test temperatures and the trend reversed at higher temperatures. The figure also shows superior strength of the zinc-based alloys comprising 11.5 and 27.5 mass% Al as compared to that of the zinc-based alloys containing 37.5 and 47.5 mass% Al when the test temperatures were low. An opposite trend was noted at higher test temperatures (Fig. 2b). Further, the extent of reduction in the strength of the zinc-based alloys decreased with their aluminum content at higher test temperatures.

Elongation of the alloys is plotted as a function of strain rate and test temperature in Fig. 3(a) and (b), respectively. An increase in strain rate improved the elongation (Fig. 3a). Moreover, the aluminum bronze attained maximum elongation (especially so at higher strain rates), whereas that of the leaded-tin bronze was lowest. Further, in the case of the zinc-based alloys, elongation values were largest for the alloy with 27.5 mass% Al followed by the alloys containing 47.5, 37.5, and 11.5 mass% Al (Fig. 3a).

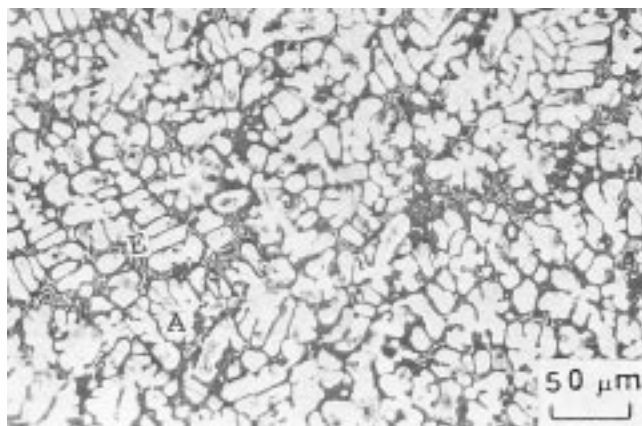
Increasing test temperature caused the elongation of the alloys to increase in general (Fig. 3b). However, in some cases, e.g., for the aluminum bronze and the zinc-based alloys with 37.5 and 47.5 mass% Al, elongation increased with temperature first, attained the maximum at a specific temperature, and decreased further at higher test temperatures. The aluminum bronze showed highest elongation, whereas the leaded-tin



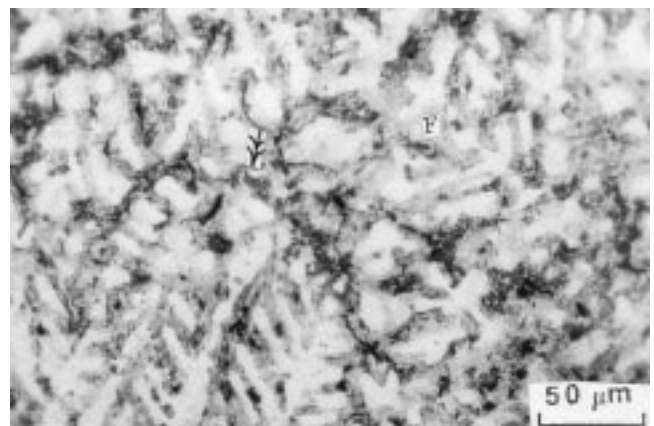
(a)



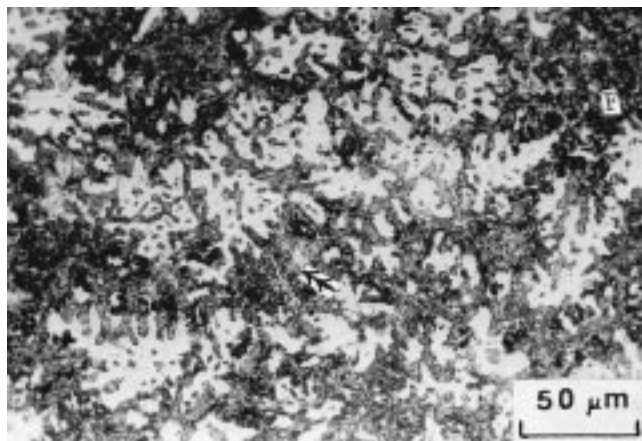
(b)



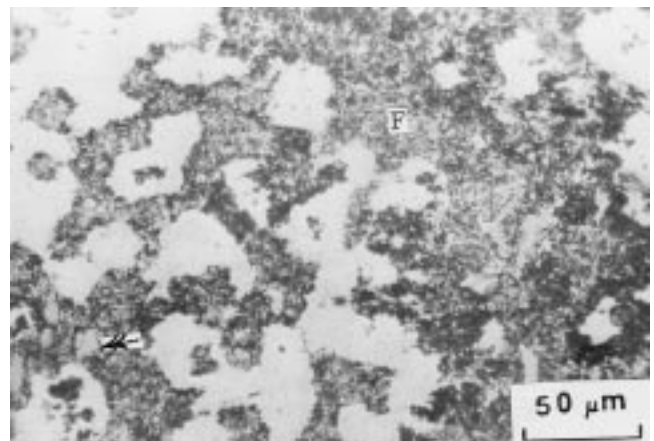
(c)



(d)



(e)



(f)

**Fig. 1** Microstructure of (a) leaded-tin bronze, (b) aluminum bronze, and (c) to (f) zinc-based alloys containing (c) 11.5 mass%, (d) 27.5 mass%, (e) 37.5 mass%, and (f) 47.5 mass% Al. A: primary  $\alpha$ , B: Cu-Sn intermetallic compound, C: lead particle, D: Cu-Al precipitate, single arrow: iron particle, E: eutectic  $\alpha + \eta$ , double arrow:  $\epsilon$ , and F: eutectoid  $\alpha + \eta$

bronze attained the lowest (Fig. 3b). The zinc-based alloys exhibited intermediate elongation. Among the zinc-based alloys, the one containing 27.5 mass% Al attained highest elon-

gation, whereas the alloys having 37.5 and 47.5 mass% Al showed lower elongation values. Further, the alloy with 11.5% Al exhibited an intermediate behavior.

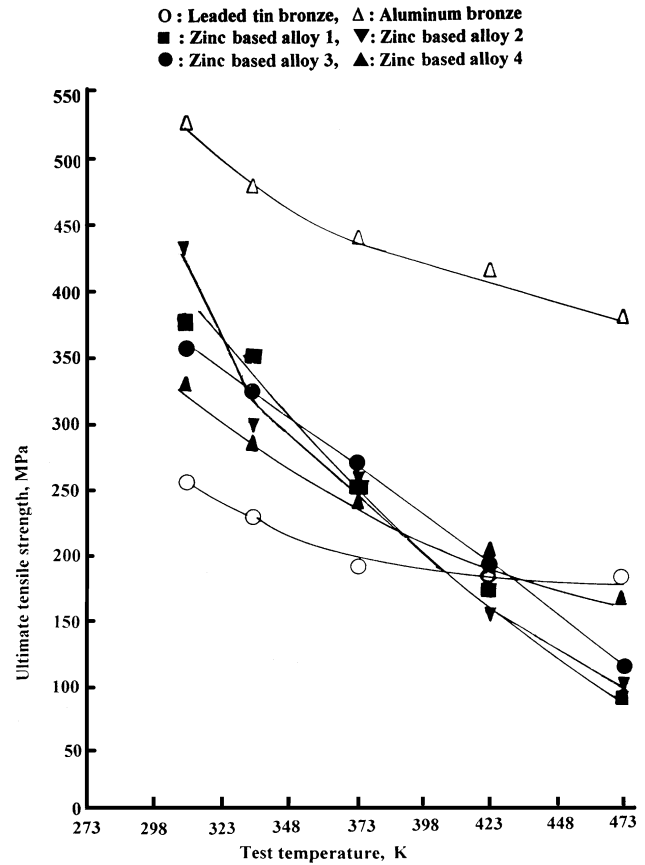
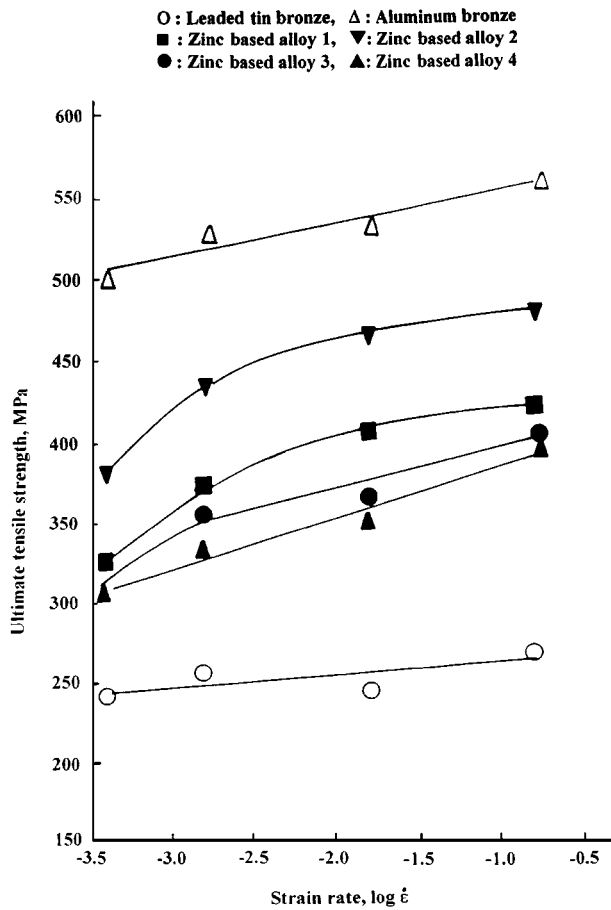


**Fig. 2** Tensile strength of the alloys plotted as a function of (a) strain rate at room temperature, *i.e.*, at 308 K and (b) test temperature at the strain rate of  $1.52 \times 10^{-3} \text{ s}^{-1}$

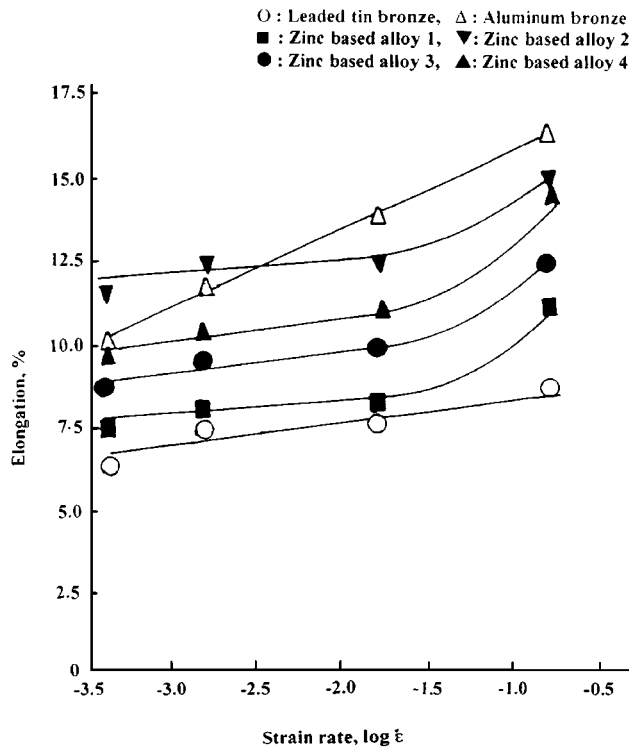
### 3.3 Fractographic Features

Figure 4 shows the fractured surfaces of the leaded-tin bronze. Room-temperature tests revealed regions indicating brittle and ductile modes of fracture (Fig. 4a). Microcracking along the lead/matrix interfacial regions was also observed (Fig. 4a, region marked by single arrow). Increasing strain rate showed a relatively larger contribution of ductile mode of fracture, as evident from more dimple formation on the fractured surface of the specimen (Fig. 4b). A typical example of the fracturing tendency of lead particles is shown in Fig. 4(c) (region marked by double arrow). Samples tested at higher temperatures exhibited larger contribution of ductile mode of fracture (Fig. 4d).

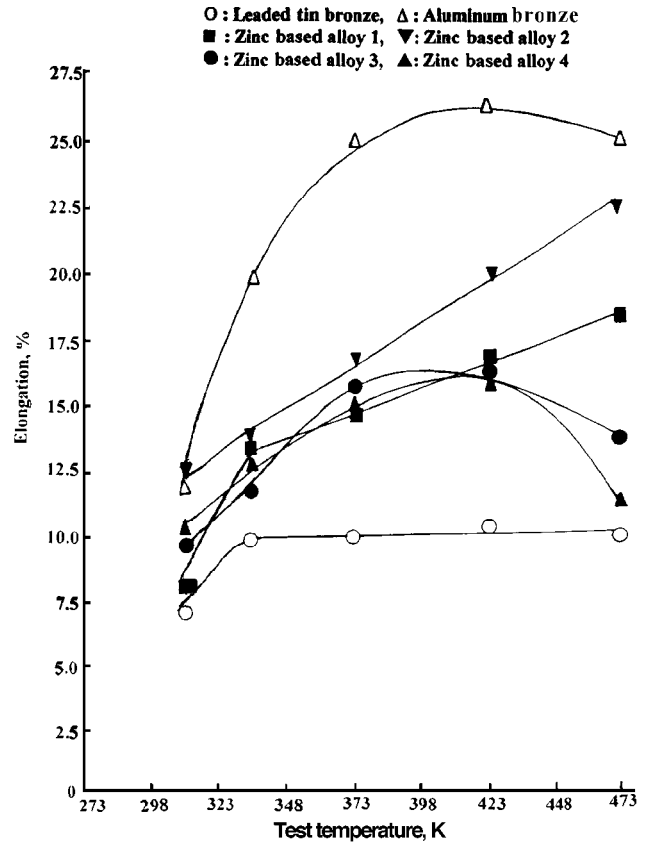
The aluminum bronze experienced both ductile and brittle modes of fracture in general (Fig. 5). Fracture along interdendritic regions was observed at low test temperatures and strain rates (Fig. 5a). A magnified view clearly shows the presence of dimples indicative of ductile fracture (Fig. 5b). Increasing strain rate reduced the tendency of the bronze toward fracturing along the interdendritic regions (Fig. 5c versus b). Marginal coarsening of dimples was noted with increasing test temperature (Fig. 5d).

Fractographic features of the zinc-based alloy containing 11.5 mass% Al were observed to be interdendritic in nature when tested at low strain rates and temperatures (Fig. 6a). Microcracking of microconstituents (such as  $\epsilon$ ) also took place in this case (Fig. 6b, arrow marked region). A higher strain rate caused the fractured surface to show a somewhat larger extent of ductile regions (Fig. 6c). The contribution of the ductile mode of fracture increased further to a great extent as the test temperature was raised (Fig. 6d through f). The dimples were noted to coarsen significantly at the maximum test temperature (Fig. 6e and f).

The zinc-based alloy comprising 47.5 mass% Al revealed fracturing along the interdendritic regions at low strain rates and temperatures (Fig. 7a). The presence of (ductile) regions containing dimples in this case could be seen in Fig. 7(b). The tendency of the alloy to fracture along selective regions decreased at higher strain rates (Fig. 7c). Testing the alloy at elevated temperatures led to the generation of an increased extent of ductile regions (Fig. 7d and e). Fracturing of microconstituents (Fig. 7d, regions marked by arrow) and coarsening of dimples at higher test temperatures (Fig. 7e versus d) were additional fractographic features of the alloy.



(a)



(b)

**Fig. 3** Tensile elongation of the alloys plotted as a function of (a) strain rate at room temperature, *i.e.*, at 308 K and (b) test temperature at the strain rate of  $1.52 \times 10^{-3} \text{ s}^{-1}$

### 3.4 Subsurface Studies

Figure 8 shows the subsurface regions of the leaded-tin bronze. Microcracks were observed in the regions near the fractured surface at low test temperatures (Fig. 8a, arrow marked region). Interfacial cracking and fracturing of microconstituents occurred at higher test temperatures (Fig. 8b, regions marked by single and double arrows, respectively).

The aluminum bronze experienced limited flow of microconstituents in the direction of tension when tests were conducted at low strain rates and temperatures (Fig. 9a). Microcracking along the Cu-Al phase/matrix interfacial regions was also observed (Fig. 9b, arrow marked region). Flow of material/microconstituents occurred to a considerable extent during elevated temperature tests (Fig. 9c). Further, the tendency of the bronze towards cracking along the interfacial regions reduced significantly under the circumstances (Fig. 9d).

In the case of the zinc-based alloy containing 11.5 mass% Al, low-temperature tests caused limited flow of material in the direction of applied tension (Fig. 10a). Also, the extent of interfacial cracking was negligibly small (Fig. 10b). Testing the samples at elevated temperatures greatly enhanced the degree of material flow (Fig. 10c).

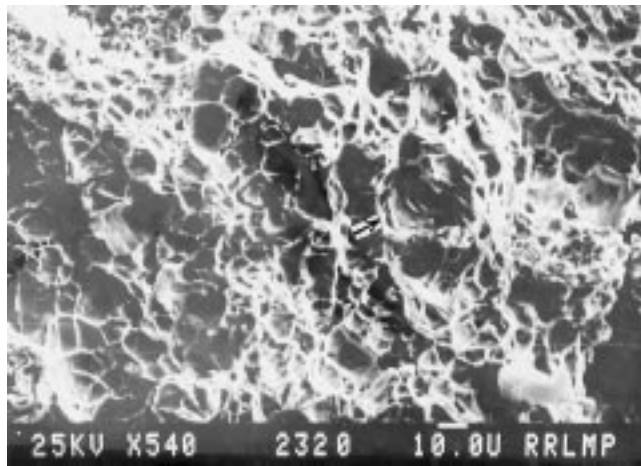
Figure 11 shows the subsurface characteristics of the zinc-based alloy comprising 47.5 mass% Al. Low-temperature tests delineated marginal flow of microconstituents (Fig. 11a). The

specimens also tended to experience interfacial cracking marginally (Fig. 11a and b, arrow marked regions). This tendency was reduced to a great extent in the case of the specimens tested at elevated temperatures (Fig. 11c).

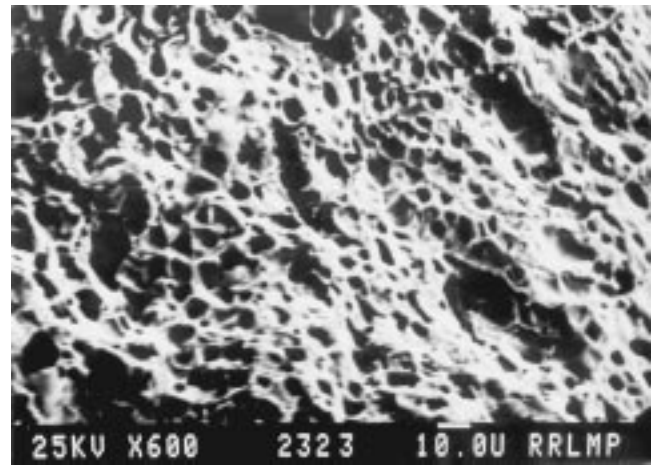
## 4. Discussion

The leaded-tin bronze comprised  $\alpha$  (a solid solution of tin in copper) and Cu-Sn intermetallic compound along with lead particles (Fig. 1a). The  $\alpha$  phase is soft and ductile, whereas the Cu-Sn compound is hard and carries load.<sup>[9-13]</sup> Lead has very limited solid solubility with copper/tin,<sup>[14,15]</sup> which causes the lead/matrix bonding to be weak.<sup>[9]</sup> Accordingly, the lead/matrix interfacial regions serve as potential sites for the nucleation and propagation of microcracks (Fig. 4a and 8). In other words, lead introduces crack sensitivity in the leaded-tin bronze. The soft lead particles also serve as voids in the alloy, such as soft dispersoid phases in metal matrix composites,<sup>[16]</sup> thereby deteriorating its strength. However, the degree of crack sensitivity reduces with an increase in temperature.<sup>[9,10,11]</sup>

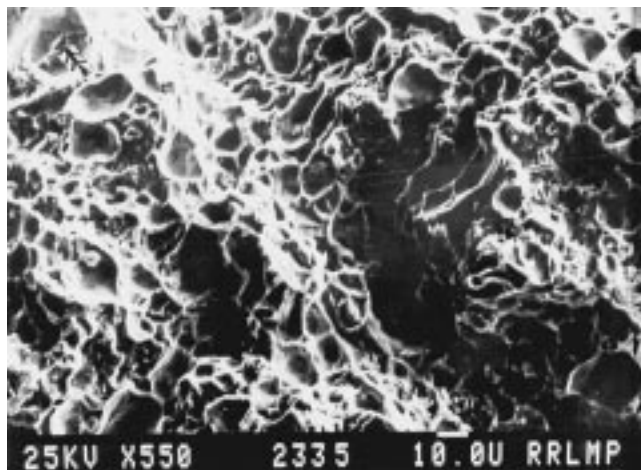
Microstructural features of aluminum bronze (Fig. 1b) showed the formation of primary  $\alpha$  (a solid solution of aluminum in copper) and Cu-Al compounds along with the particles of iron.<sup>[10]</sup> In this case, the  $\alpha$  phase is soft, whereas the remaining



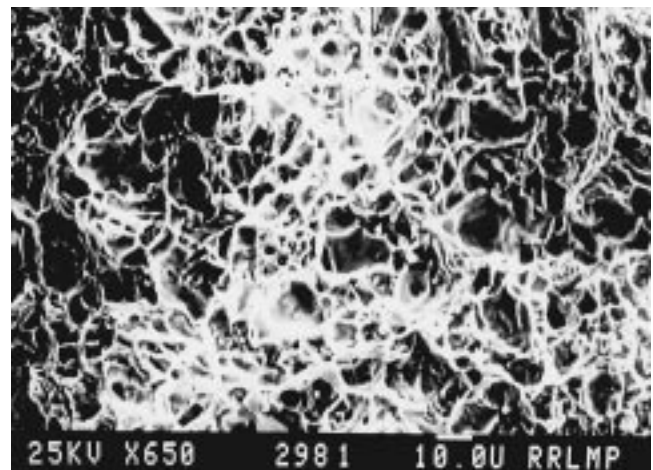
(a)



(b)



(c)



(d)

**Fig. 4** Fractographic features of the leaded-tin bronze tested at (a) 308 K at  $1.52 \times 10^{-3} \text{ s}^{-1}$ , (b) and (c) 308 K at  $1.52 \times 10^{-2} \text{ s}^{-1}$ , and (d) 473 K at  $1.52 \times 10^{-3} \text{ s}^{-1}$ . Single arrow: lead/matrix interfacial cracking; and double arrow: fracturing of lead particle

microconstituents are harder and carry load.<sup>[10]</sup> The alloy has lower crack sensitivity than the leaded-tin bronze (Fig. 9 versus 8) in the absence of any crack-sensitive phase (such as lead in the leaded-tin bronze). The extent of cracking decreases further with temperature (Fig. 9c and d versus 9a and b).

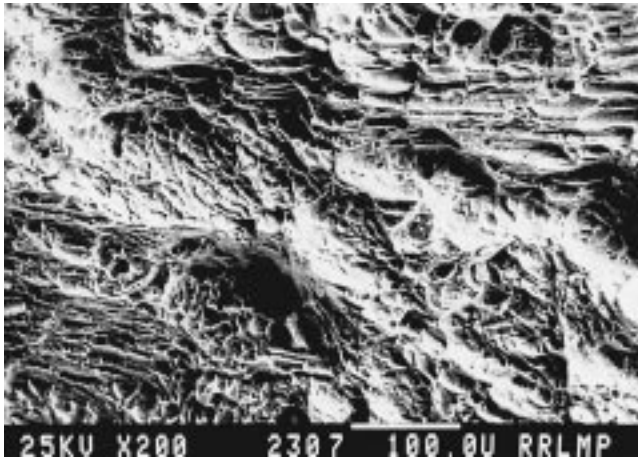
Zinc-based alloys in general comprised a mixture of ( $\alpha$  and  $\eta$ ) solid solutions along with (a minor quantity of) the metastable  $\varepsilon$  phase distributed in a specific manner (Fig. 1c through f). Both  $\alpha$  and  $\eta$  (the major microconstituents of the alloy system) are soft and ductile in nature and carry load.<sup>[12,13,17]</sup> These alloys also do not contain crack-sensitive phases (such as lead in the leaded-tin bronze). Also, the zinc-based alloys have a lower melting point than either of the bronzes.<sup>[12]</sup>

The response of the alloys under tensile loading conditions can be explained in terms of their thermal stability and cracking tendency (*i.e.*, crack sensitivity). Here, the term “thermal stability” indicates the ability of the samples to retain their strength at elevated temperatures to a larger extent. Accordingly, alloys having better thermal stability attained superior strength property at high temperatures (Fig. 2b). Needless to say, thermal stability is directly proportional to the melting point of the alloy

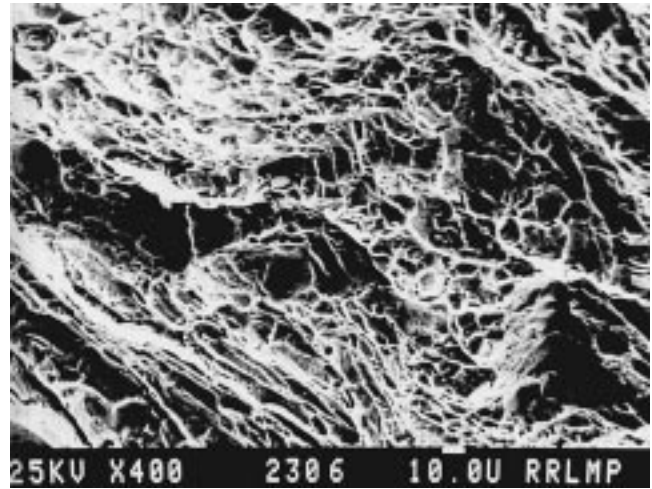
system. From a thermal stability point of view, the aluminum bronze ranks the best, followed by the leaded-tin bronze and the zinc-based alloys. However, the leaded-tin bronze suffers from cracking tendency to the largest extent (Fig. 8), whereas the zinc-based alloys exhibit the minimum (Fig. 10 and 11). The aluminum bronze shows intermediate cracking tendency (Fig. 9).

Strain hardening and microcracking characteristics greatly control the tensile properties of materials.<sup>[18,19]</sup> Strain hardening arises due to increased dislocation density during the process of deformation<sup>[18]</sup> and leads to superior tensile properties. Increasing strain rate (within limits) improves the tensile properties of materials.<sup>[18–24]</sup> On the other hand, the microcracking tendency of a material produces a reverse effect.<sup>[18,19]</sup> Factors such as inclusions, microporosity, weaker/poorly compatible phases, as well as stress raiser points enhance the microcracking tendency of materials.<sup>[18]</sup> Thus, the overall performance of a material would depend on the net effect of the mentioned factors, *i.e.*, strain hardening and microcracking characteristics under a given set of test conditions.

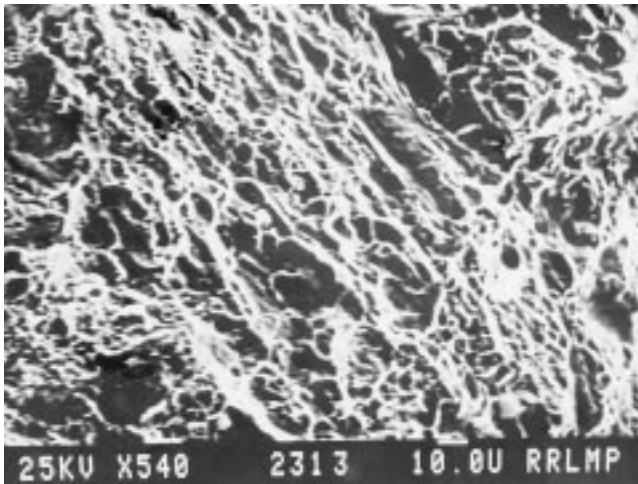
Low strain rates involving low cross-head speeds cause the



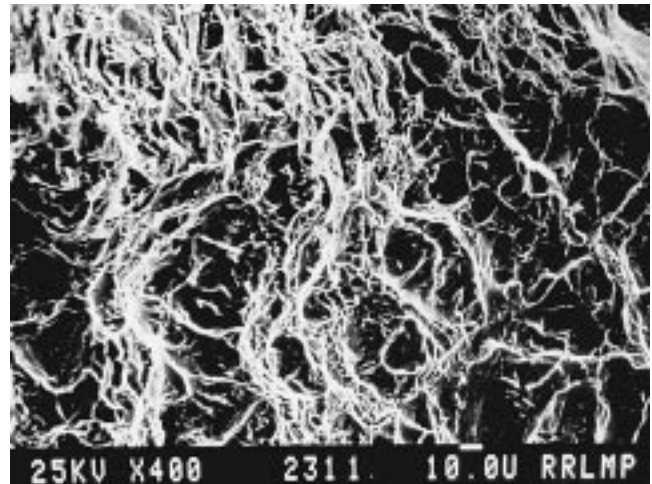
(a)



(b)



(c)



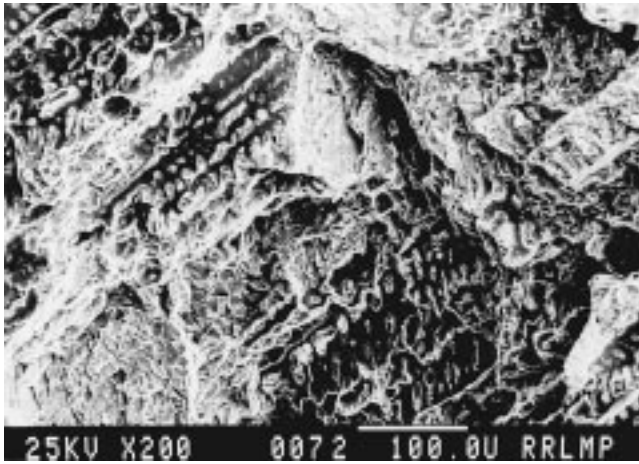
(d)

**Fig. 5** Fractographs of the aluminum bronze tested at (a) and (b) 308 K at  $1.52 \times 10^{-3} \text{ s}^{-1}$ , (c) 308 K at  $1.52 \times 10^{-2} \text{ s}^{-1}$ , and (d) 473 K at  $1.52 \times 10^{-3} \text{ s}^{-1}$

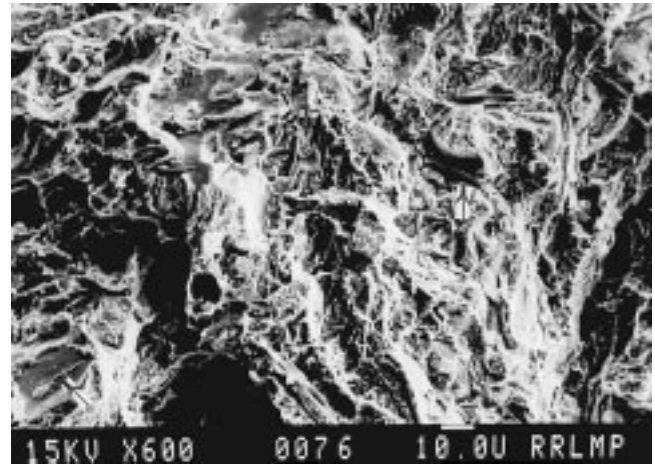
applied stress to be effective over a wider gauge area. As a result, all the (weak/strong) phases/regions contribute to control the mechanical properties of the alloys, wherein the negative influences of the constituent phases also are reflected during testing (Fig. 5a, 6a, and 7a). On the other hand, when the strain rate is high, the stress raiser points, weaker/crack sensitive constituents/regions do not get enough time to participate in load transfer or crack nucleation/propagation and, hence, to adversely affect the properties of the samples, since the applied load is mainly shared by the stronger regions/phases.<sup>[18]</sup> This was also evident from the presence of an increased extent of ductile regions on the fractured surfaces of the samples tested at larger strain rates (Fig. 5c versus 5a and b, 6c versus 6b, and 7c versus 7a). Accordingly, the tensile properties improved with strain rate (Fig. 2a and 3a). A varying degree of the effectiveness of strain rate on the tensile properties of the alloys could be attributed to the extent to which the negative effects of the phases/regions predominated their load carrying and deformability characteristics.

Increasing temperature improves the (plastic) deformability of the alloys while their crack sensitivity decreases (Fig. 9c and d versus 9a and b, 10c versus a, and 11c versus a). As a result, the strength of the alloys decreased, whereas their elongation improved with temperature (Fig. 2b and 3b). A reduction in elongation in some cases beyond a specific test temperature may be due to a high rate of softening causing catastrophic failure under the circumstances.

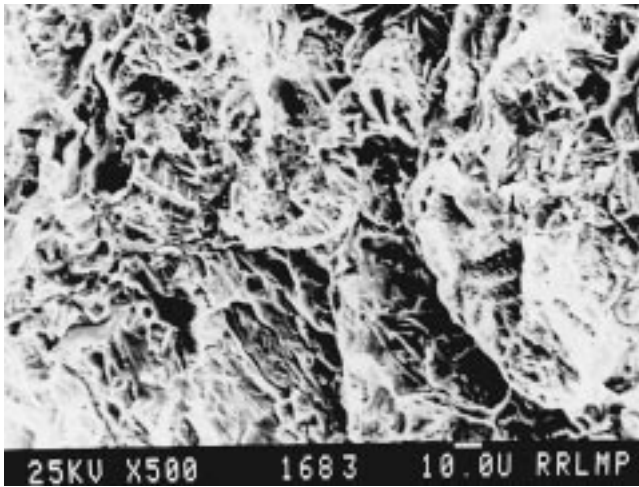
Most superior tensile properties of the aluminum bronze (Fig. 2 and 3) could result from a stronger matrix and considerably lower microcracking tendency (Fig. 5 and 9) of its constituent phases (Fig. 1b). On the other hand, the predominating microcracking nature of the leaded-tin bronze (Fig. 8) due to the presence of discrete particles of practically insoluble lead (Fig. 1a) caused its tensile properties to be the most inferior (Fig. 2 and 3). The properties of the zinc-based alloys were intermediate between the two bronzes. This was due to the lower cracking tendency of the zinc-based alloys (compared to the leaded-tin bronze, Fig. 10 versus 8) and inferior thermal



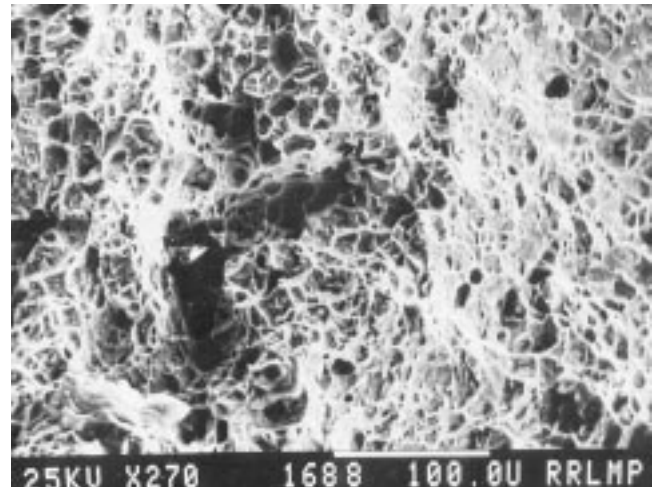
(a)



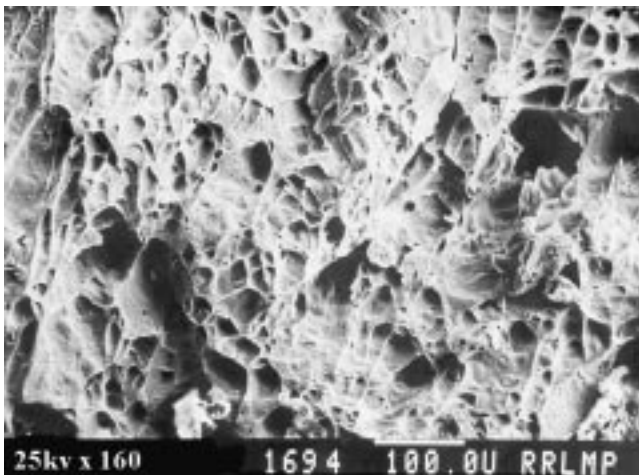
(b)



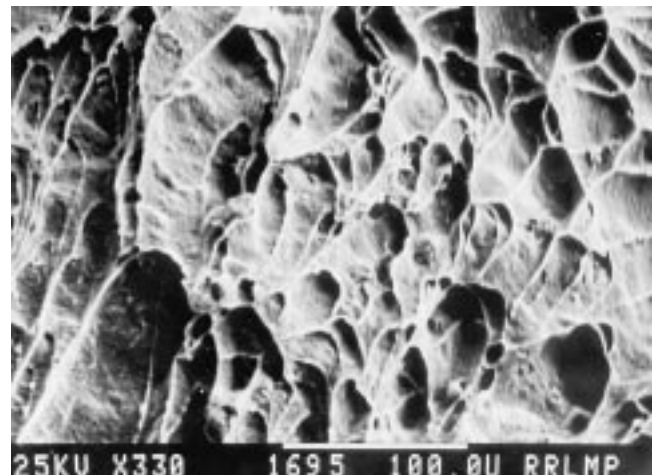
(c)



(d)

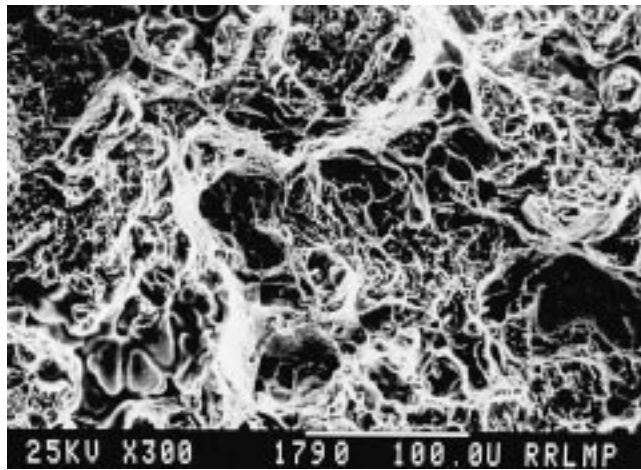


(e)

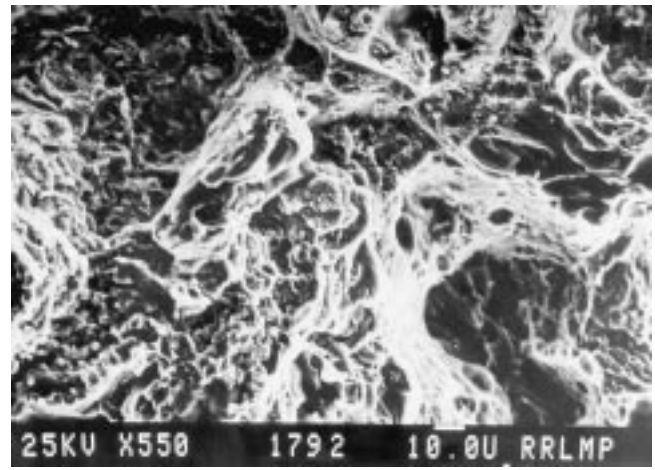


(f)

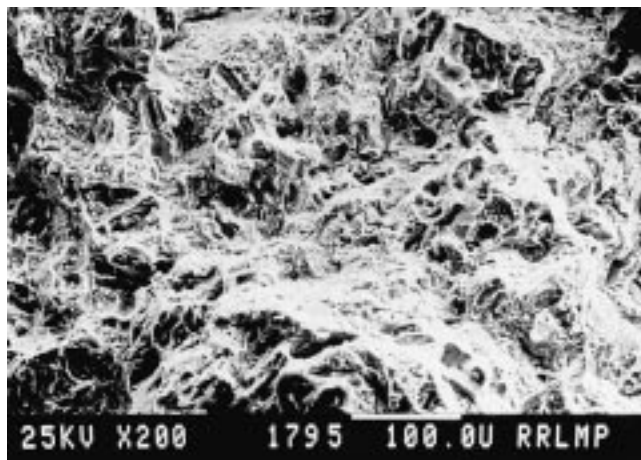
**Fig. 6** Fractured surfaces of the zinc-based alloy containing 11.5 mass% Al tested at (a) and (b) 308 K at  $1.52 \times 10^{-3} \text{ s}^{-1}$ , (c) 308 K at  $1.52 \times 10^{-2} \text{ s}^{-1}$ , (d) 373 K at  $1.52 \times 10^{-3} \text{ s}^{-1}$ , and (e) and (f) 473 K at  $1.52 \times 10^{-3} \text{ s}^{-1}$ . Arrow: microcracking of microconstituents



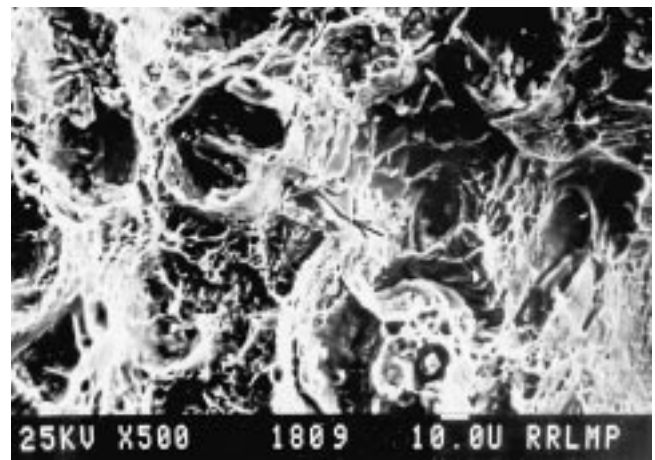
(a)



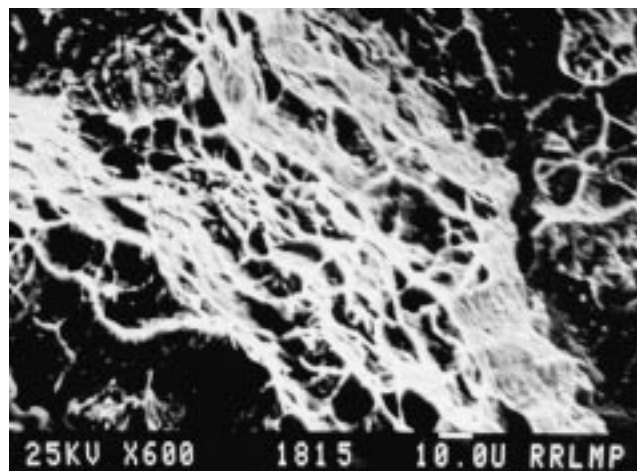
(b)



(c)



(d)

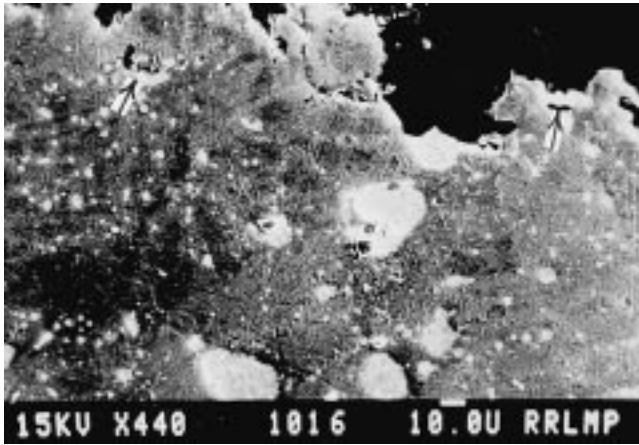


(e)

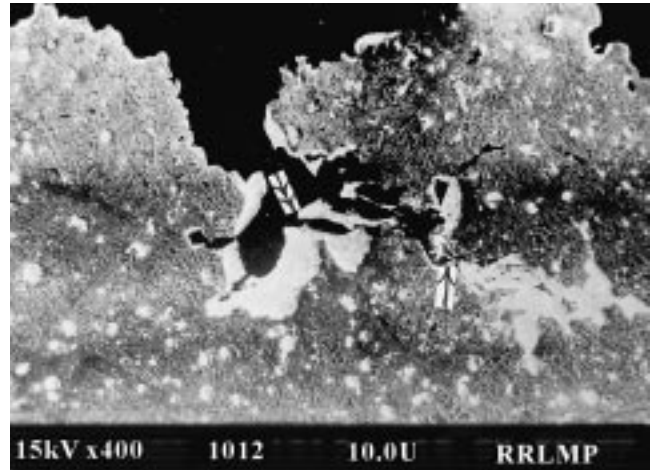
**Fig. 7** Fractographs of the zinc-based alloy containing 47.5 mass% Al tested at (a) and (b) 308 K at  $1.52 \times 10^{-3} \text{ s}^{-1}$ , (c) 308 K at  $1.52 \times 10^{-2} \text{ s}^{-1}$ , (d) 373 K at  $1.52 \times 10^{-3} \text{ s}^{-1}$ , and (e) 473 K at  $1.52 \times 10^{-3} \text{ s}^{-1}$ . Arrow: fracturing of microconstituents

stability (compared to that of the aluminum bronze, as evident from more coarsening of dimples on fractured surfaces, Fig. 6d and e versus 5d, and more material flow for the zinc-based

alloys, Fig. 10c versus 9(c)). Superior thermal stability of the Cu matrix in the leaded-tin bronze led to its higher tensile strength at elevated temperatures as compared to the zinc-based



(a)

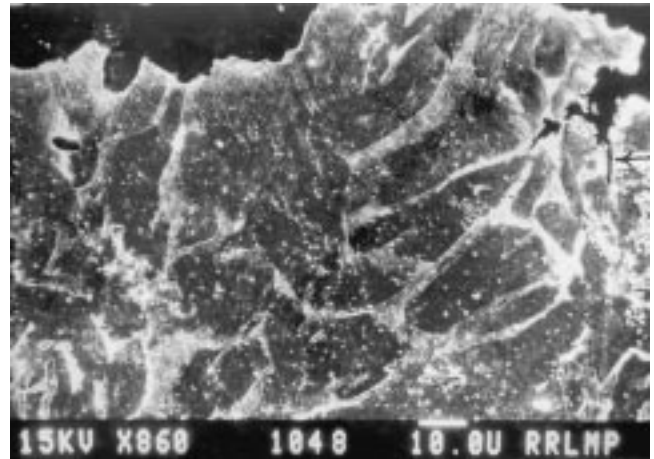


(b)

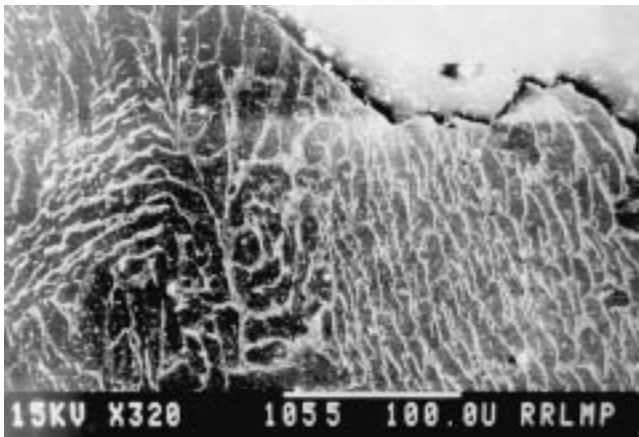
**Fig. 8** Subsurface regions of the leaded-tin bronze tested at the strain rate of  $1.52 \times 10^{-3} \text{ s}^{-1}$  at (a) 308 K and (b) 473 K. Single arrow: interfacial cracking, and double arrow: cracking of lead particle



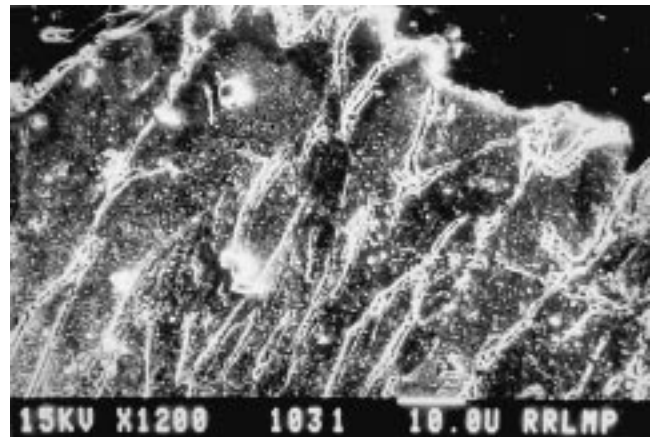
(a)



(b)

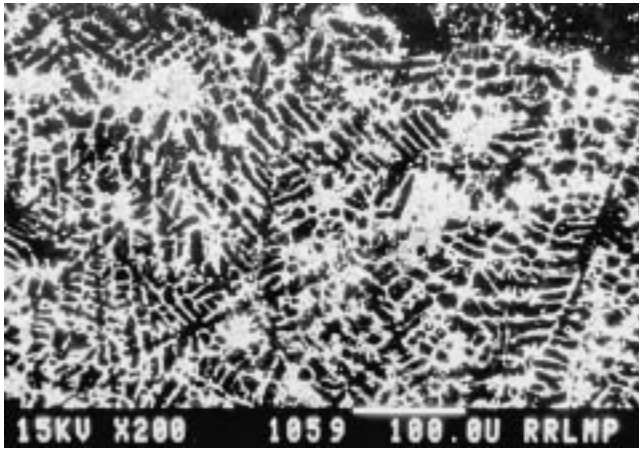


(c)

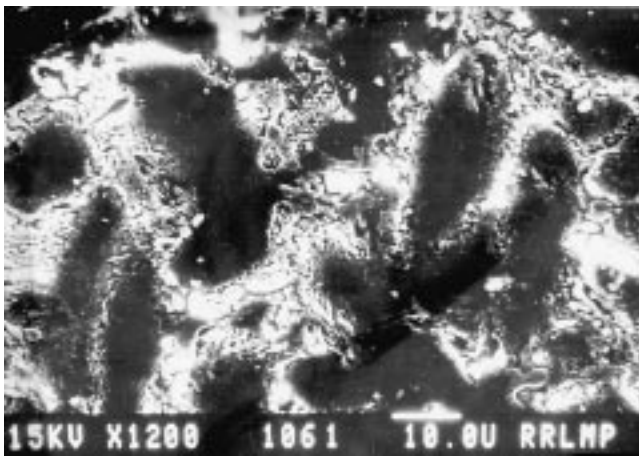


(d)

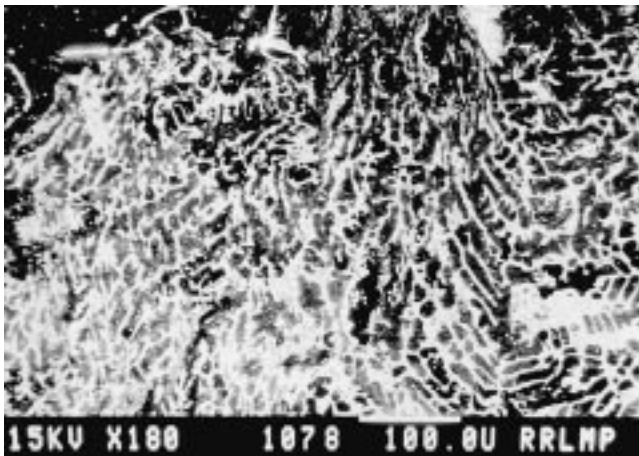
**Fig. 9** Subsurface properties of the aluminum bronze tested at the strain rate of  $1.52 \times 10^{-3} \text{ s}^{-1}$  at (a) and (b) 308 K and (c) and (d) 473 K. Arrow: interfacial cracking



(a)



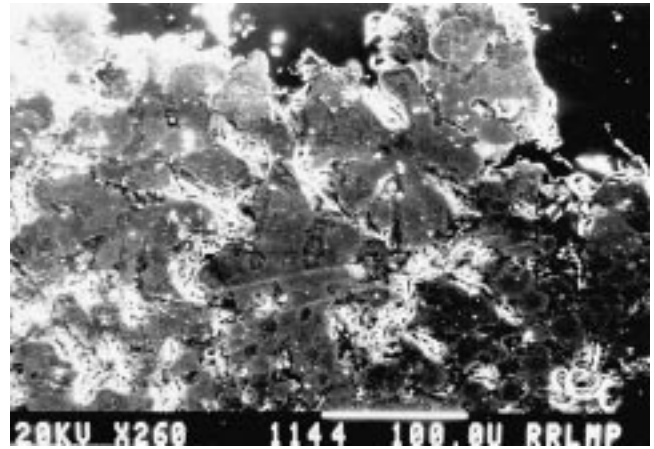
(b)



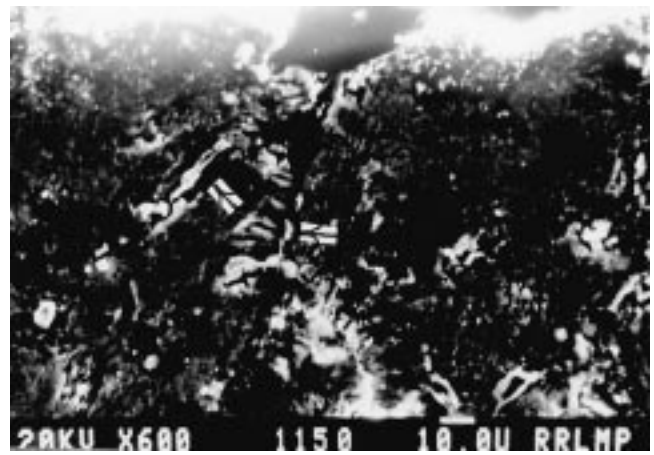
(c)

**Fig. 10** Micrographs showing the subsurface features of the zinc-based alloy containing 11.5 mass% Al tested at the strain rate of  $1.52 \times 10^{-3} \text{ s}^{-1}$  at (a) and (b) 308 K and (c) 473 K

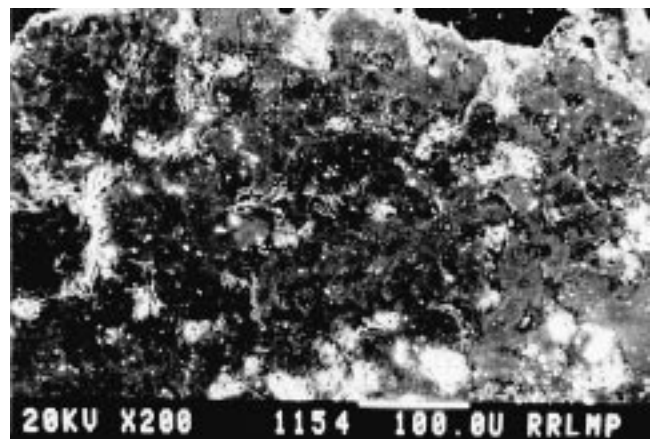
alloys (Fig. 2b). Further, better thermal stability imparted by the relatively high-melting aluminum led to superior strength of the zinc-based alloys with higher concentrations of the ele-



(a)



(b)



(c)

**Fig. 11** Subsurface characteristics of the zinc-based alloy containing 47.5 mass % Al tested at the strain rate of  $1.52 \times 10^{-3} \text{ s}^{-1}$  at (a) and (b) 308 K and (c) 473 K. Arrow: interfacial cracking

ment at elevated test temperatures (Fig. 2b). The element also reduced the extent of deterioration in the strength of the zinc-based alloys with temperature (Fig. 2b) for the same reason.

Better thermal stability of the zinc-based alloy containing a greater quantity of aluminum is evident from the reduced extent of coarsening of dimples (Fig. 7d and e versus 6d through f) and less material flow in the direction of tension (Fig. 11c versus 10c). Further, superior tensile properties of the zinc-based alloy having 27.5 mass% Al than the remaining varieties of the zinc-based alloys (Fig. 2 and 3) could be attributed to the aluminum concentration of the former to be nearer to that of the eutectoid composition forming at 22 mass% Al;<sup>[25]</sup> eutectoid zinc-aluminum alloys attain superplasticity.<sup>[20–24]</sup>

An appraisal of the observations made in this study suggests that important factors controlling the tensile properties of the alloys include thermal stability, microcracking tendency, and deformability characteristics. An optimum level of contribution from the factors (excluding the crack sensitivity property, which certainly must be the least to attain good tensile characteristics) could lead to superior strength and elongation. However, the predominance of the effects of the factors is governed to a great extent by the test conditions. As a result, the response of the alloys varied with the conditions under which tests were conducted. It is also obvious that a series of zinc-based alloys with different combinations of tensile properties can be developed by controlling their aluminum contents.

## 5. Conclusions

- The aluminum bronze exhibited highest tensile strength and elongation and those of the leaded-tin bronze were the least. The zinc-based alloys showed their properties to be intermediate between the two.
- Among the zinc-based alloys, the one with 27.5 mass% Al attained best tensile properties and the ones containing higher amounts of aluminum exhibited superior strength at elevated test temperatures. The leaded-tin bronze showed better strength than the zinc-based alloys at higher temperatures and the trend reversed at low test temperatures.
- Tensile strength increased with strain rate, whereas temperature had a reverse effect. On the other hand, elongation of the alloys improved with strain rate and test temperature.
- Factors controlling the tensile properties of the alloys were observed to be their thermal stability, capability to undergo plastic deformation, and their crack sensitivity. Contribution of such factors, of course, varied with the test conditions.

- It is possible to develop zinc-based alloys with different combinations of tensile properties through compositional alterations. The alloys could find utility in different engineering applications in place of bronzes.

## References

1. *Metals Handbook*, 1st ed., ASM, Materials Park, OH, 1992, vol. 18, pp. 515-22.
2. G.C. Pratt: *Int. Met. Rev.*, 1973, vol. 18, pp. 1-27.
3. *Copper and Its Alloys*, E.G. West, ed., Ellis Horwood Publishers, Chichester, Sussex, England, 1982, pp. 84-131.
4. *Metals Handbook*, 9th ed., ASM, Materials Park, OH, 1979, vol. 2, pp. 383-94.
5. *Zinc and Its Alloys and Compounds*, 1st ed., S.W.K. Morgan, ed., Ellis Horwood Publisher, Chichester, Sussex, England, 1985, pp. 154-64.
6. E.J. Kubel Jr.: *Adv. Mater. Processing*, 1987, vol. 132, pp. 51-57.
7. B.K. Prasad, A.K. Patwardhan, and A.H. Yegneswaran: *Z. Metallkd.*, 1996, vol. 87, pp. 967-72.
8. B.K. Prasad, A.K. Patwardhan, and A.H. Yegneswaran: *J. Mater. Sci.*, 1996, vol. 1, pp. 6317-24.
9. B.K. Prasad, A.K. Patwardhan, and A.H. Yegneswaran: *Mater. Sci. Technol.*, 1996, vol. 12, pp. 427-35.
10. B.K. Prasad: *Metall. Mater. Trans. A*, 1997, vol. 28A, pp. 809-15.
11. B.K. Prasad, A.K. Patwardhan, and A.K. Yegneswaran: *Metall. Mater. Trans. A*, 1996, vol. 27A, pp. 3513-23.
12. B.K. Prasad, A.K. Patwardhan, and A.H. Yegneswaran: *Z. Metallkd.*, 1997, vol. 88, pp. 774-80.
13. J.P. Pandey, B.K. Prasad, and A.H. Yegneswaran: *Mater. Trans. JIM*, 1998, vol. 39, pp. 1121-25.
14. W.A. Glaeser: *Proc. Int. Conf. on Wear of Materials*, K.C. Ludema, ed., ASME, New York, NY, 1989, vol. 1, pp. 255-60.
15. *Friction and Wear of Materials*, E. Rabinowicz, ed., John Wiley and Sons, New York, NY, 1965, pp. 84-131.
16. B.S. Mazumdar, A.H. Yegneswaran, and P.K. Rohatgi: *Mater. Sci. Eng.*, 1984, vol. 68, pp. 85-96.
17. S. Murphy and T. Savaskan: *Wear*, 1984, vol. 98, pp. 151-61.
18. B.K. Prasad, A.K. Patwardhan, and A.H. Yegneswaran: *J. Mater. Sci.*, 1997, vol. 32, pp. 1169-75.
19. T.S. Srivatsan, S. Anand, and T.S. Sudarshan: *Mater. Sci. Technol.*, 1996, vol. 10, pp. 640-46.
20. T. Hikosaka, T. Imai, T.G. Nieh, and J. Wadsworth: *Scripta Metall.*, 1994, vol. 31, pp. 1181-86.
21. S. Mitra: *J. Mater. Sci. Lett.*, 1994, vol. 13, pp. 1296-1300.
22. F.A. Mohammed, M.M.I. Ahmed, and T.G. Langdon: *Metall. Trans. A*, 1977, vol. 8A, pp. 933-38.
23. J.W. Bowden and B. Ramaswami: *Metall. Trans. A*, 1990, vol. 21A, pp. 2497-2504.
24. M.M.I. Ahmed, F.A. Mohammed, and T.G. Langdon: *J. Mater. Sci.*, 1979, vol. 14, pp. 2913-21.
25. Brandes, E.A., ed.: *Smithells Metals Reference Book*, 6th ed., Butterworth and Co., London, 1983, pp. 370-801.